

# Structure and DNA-binding properties of the *Bacillus subtilis* SpoIIIE DNA translocase revealed by single-molecule and electron microscopies

Diego I. Cattoni, Shreyasi Thakur, Cedric Godefroy, Antoine Le Gall, Josephine Lai-Kee-Him, Pierre-Emmanuel Milhiet, Patrick Bron and Marcelo Nöllmann\*

Centre de Biochimie Structurale, Department of Single-Molecule Biophysics CNRS UMR5048, INSERM U554, Université de Montpellier I & II, 29 rue de Navacelles, 34090 Montpellier, France

Received July 14, 2013; Revised October 29, 2013; Accepted November 6, 2013

## ABSTRACT

SpoIIIE/FtsK are a family of ring-shaped, membrane-anchored, ATP-fuelled motors required to segregate DNA across bacterial membranes. This process is directional and requires that SpoIIIE/FtsK recognize highly skewed octameric sequences (SRS/KOPS for SpoIIIE/FtsK) distributed along the chromosome. Two models have been proposed to explain the mechanism by which SpoIIIE/FtsK interact with DNA. The loading model proposes that SpoIIIE/FtsK oligomerize exclusively on SpoIIIE recognition sequence/orienting polar sequences (SRS/KOPS) to accomplish directional DNA translocation, whereas the target search and activation mechanism proposes that pre-assembled SpoIIIE/FtsK hexamers bind to non-specific DNA, reach SRS/KOPS by diffusion/3d hopping and activate at SRS/KOPS. Here, we employ single-molecule total internal reflection imaging, atomic force and electron microscopies and ensemble biochemical methods to test these predictions and obtain further insight into the SpoIIIE–DNA mechanism of interaction. First, we find that SpoIIIE binds DNA as a homo-hexamer with neither ATP binding nor hydrolysis affecting the binding mechanism or affinity. Second, we show that hexameric SpoIIIE directly binds to double-stranded DNA without requiring the presence of SRS or free DNA ends. Finally, we find that SpoIIIE hexamers can show open and closed conformations in solution, with open-ring conformations most likely resembling a state poised to load to non-specific, double-stranded DNA. These results suggest how SpoIIIE and related ring-shaped motors may be split open to bind topologically closed DNA.

## INTRODUCTION

Several key DNA metabolic processes, such as DNA replication, transcription and segregation, require the rapid and precise movement of DNA, which is orchestrated by adenosine triphosphate (ATP)-fuelled motor proteins. *Bacillus subtilis* SpoIIIE and *Escherichia coli* FtsK are highly homologous motors responsible for the transfer of chromosomal DNA during cell division and sporulation. SpoIIIE and FtsK are able to translocate DNA rapidly both *in vitro* [4–7 kb/s at room temperature (1–3) and 17 kb/s at 37°C (4)] and *in vivo* [500 bp/s at 30°C (3)]. In sporulating *B. subtilis*, three steps are necessary for the newly replicated chromosome to be completely segregated into the forespore. First, segments of the sister chromosomes centered on the origin of DNA replication (*oriC*) are separated and attached to the poles of the cell. This process involves remodelling of the sister chromosomes into elongated axial filaments and segregation and attachment of a centromere-like element located close to *oriC* by the action of at least four proteins (Soj, Spo0J, RacA and DivIVA) (5–7). Second, expression of sporulation-specific proteins directs the asymmetric relocation of the divisional plane from its normal mid-cell locus to the vicinity of the cell pole. This newly located division septum traps about one-third of the chromosome in the forespore (Figure 1A). Third, the DNA translocase SpoIIIE localizes to future sites of septation before the onset of septal constriction and is transported by the leading edge of the closing septum until it encounters DNA (8). Next, directional DNA translocation leads to the formation of a compartment-specific complex that rapidly translocates the remainder of the chromosome (~3 Mb) through an aqueous pore into the forespore by using the energy of ATP hydrolysis (8–12) (Figure 1B).

SpoIIIE and FtsK are composed of three domains: a ~200-residue N-terminal transmembrane-spanning domain, a poorly conserved and putatively unstructured linker and a ~537-residue C-terminal domain (Figure 1B).

\*To whom correspondence should be addressed. Tel: +33 4 67 41 79 12; Fax: +33 4 67 41 79 13; Email: marcelo.nollmann@cbs.cnrs.fr

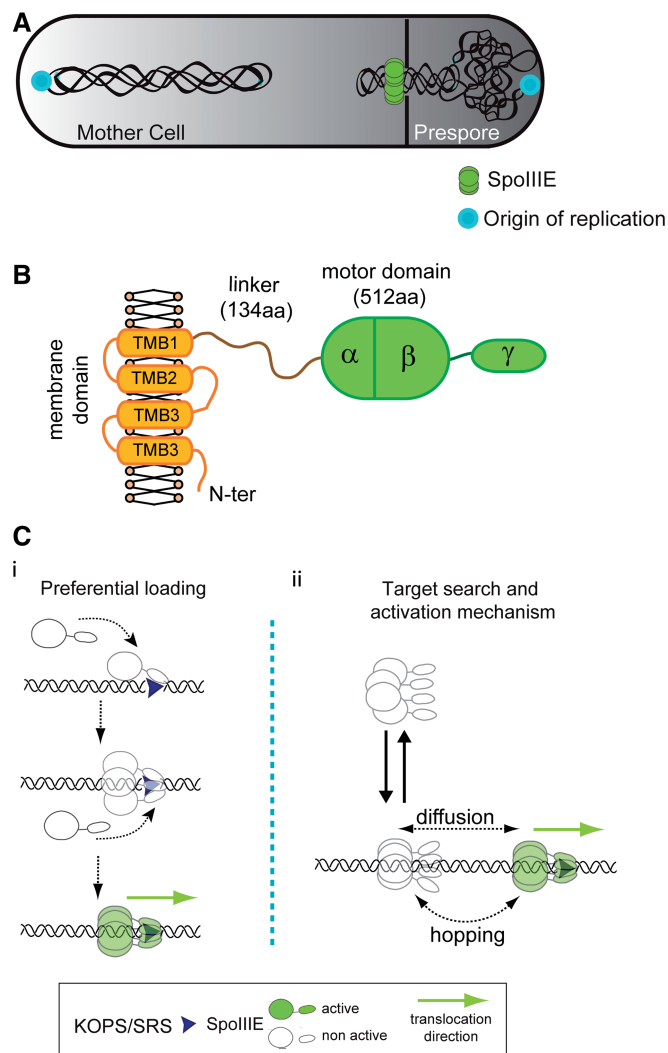


**Figure 1.** (A) Chromosome segregation in sporulating *B. subtilis*. During the initial stages of sporulation, the *oriC* regions (circles) move towards the cell poles. Immediately after, asymmetric division results in the trapping of one-third of the chromosome in the pre-spore, while the rest remains in the mother cell. SpoIIIE (dark gray circles) is recruited to the septum and translocates the remaining two-thirds of the chromosome from the mother cell to the pre-spore. (B) SpoIIIE is composed of a membrane-spanning domain (cylinders), an unstructured linker (ribbon) and a motor domain. The motor consists of hexamers of domain  $\alpha\beta$  (gray circles), with the  $\gamma$  domain (gray ellipses) implicated in SRS recognition. A single-membrane bi-layer is represented by yellow circles and black sticks (13). (C) i-Scheme representing the preferential loading model. In this model, the FtsK/SpoIIIE hexameric motor assembles exclusively at KOPS/SRS sequences. Single monomers of FtsK/SpoIIIE (white) will bind, in a six-step sequential mechanism, to KOPS/SRS (triangle) and form an active sequence-oriented hexamer (dark gray) (14). ii- Schematic representation of the target search and activation model. In this model, pre-formed SpoIIIE hexamers (white) bind non-specifically to DNA and find SRS by diffusion/3d-hopping with ensuing sequence-specific activation of the motor mediated by binding and oligomerization of SpoIIIE- $\gamma$  on SRS (dark gray).

The hydrophobic N-terminal domain of SpoIIIE contains four transmembrane domains and is both necessary and sufficient for septal localization and anchoring (9,15–18). The unstructured linker is implicated in direct interactions with other division proteins (19,20) and the C-terminal motor domain is involved in double-stranded DNA

(dsDNA) translocation (3). The SpoIIIE/FtsK motor assembles as a hexameric ring that binds dsDNA through its central channel and is composed of three separate subdomains:  $\alpha$ ,  $\beta$  and  $\gamma$  (12,14,21), with  $\alpha$  and  $\beta$  being responsible for DNA translocation and ATP hydrolysis (12,22). Genetics, bioinformatics and single-molecule methods identified the presence of highly skewed 8-bp motifs along the chromosomal arms of *B. subtilis* and *E. coli* that switch direction at dif (deletion-induced filamentation site), and demonstrated that SpoIIIE/FtsK can recognize these sequences in an orientation-specific manner (3,21,22). The sequences were named SRS for SpoIIIE [SpoIIIE recognition sequence, GAGAAGGG (3)] and KOPS for FtsK [FtsK orienting polar sequences, GGGNAGGG (23,24)].

Two models proposed to explain the molecular mechanism by which SpoIIIE/FtsK interact with DNA are depicted in Figure 1C. The preferential loading model proposes that SpoIIIE/FtsK monomers assemble specifically and with orientation specificity at SRS/KOPS sequences (14,25,26). In contrast, the target search and activation mechanism proposes that pre-assembled SpoIIIE/FtsK hexamers bind to non-specific DNA and reach SRS/KOPS by diffusion/3d-hopping, where they get activated in an orientation-specific manner (27). Here, we directly test different predictions of these models by employing single-molecule total internal reflection (TIRF) microscopy, atomic force microscopy (AFM), electron microscopy (EM) and equilibrium binding measurements. Our results indicate that: (i) in the absence of SRS, SpoIIIE can bind DNA non-specifically, (ii) in the presence of ATP, SpoIIIE becomes active and efficiently translocates on DNA devoid of SRS until reaching the end of DNA, (iii) ATP binding and hydrolysis do not affect the binding mechanism nor the affinity of SpoIIIE for DNA and (iv) SpoIIIE exists as open and closed hexamers in solution. These data suggest a binding mechanism that does not involve threading through DNA ends or sequential assembly of monomers but rather the binding of a pre-formed open hexamer with ensuing closure of the hexamer leading to a translocation-competent motor complex. These results considerably support the target search mechanism and allow us to explain the mechanism of binding of pre-formed hexamers to dsDNA.

## MATERIALS AND METHODS

### SpoIIIE purification, labelling and buffers

SpoIIIE expression constructs were derived from pJB103 (12), which contains the C-terminal motor domain of SpoIIIE (residues 177–787) with a C-terminal hexahistidine tag. Briefly, SpoIIIE and SpoIIIE<sup>467</sup> mutant were expressed in *E. coli* DH5 $\alpha$  cells by addition of anhydrotetracycline (4  $\mu$ g/ml). Cells were harvested and the tagged protein was purified by affinity chromatography on Ni<sup>2+</sup>-agarose resin (HisTrap FF, GEHealthcare Bio-Sciences, Uppsala, Sweden). Pure fractions (>90% purified by sodium dodecyl sulphate-polyacrylamide gel electrophoresis (SDS-PAGE) and coomassie blue staining) were pooled, dialysed in storage

buffer [50 mM HEPES, 150 mM NaCl, 30% (v/v) glycerol, pH 7.5] and quantified using the Bradford method.

For TIRF imaging, SpoIIIE was N-terminal, covalently labelled with Atto647N mono NHS-ester dye (Amersham Biosciences, Sunnyvale, USA) to produce SpoIIIE-Atto647N (or SpoIIIE\*). A 50-fold molar excess of the dye was added drop-by-drop to a solution of purified SpoIIIE and the reaction was allowed to proceed at 4°C for 1 h with continuous agitation. The reaction buffer was 50 mM HEPES, pH 7.5, 250 mM NaCl, 5% glycerol. The reaction was stopped by adding 10% v/v 1 M Tris-HCl pH 7.5. The free unreacted dye was removed by dialysis against the reaction buffer in absence of free dye. The ratio of labelling was estimated using the extinction coefficient of the dye provided by the supplier ( $1.5 \times 10^5$  M/cm at 644 nm) and the protein concentration was measured by the Bradford assay. By this method, the degree of labelling was found to be 25–30%. This modification did not affect the ATPase activity of SpoIIIE. At least three independent preparations of purified SpoIIIE were evaluated for each experiment.

Measurements of SpoIIIE binding and ATPase activity were performed in reaction buffer (50 mM Tris, pH 7.5, 0.15 mg/ml bovine serum albumin, 3% Glycerol, 7.5 mM NaCl and 10 mM MgCl<sub>2</sub>). All chemicals used in this work were of analytical grade.

### Sodium dodecyl sulphate–polyacrylamide gel electrophoresis

SDS-PAGE gels were run with a Hoefer minigel device (Holliston, USA) according to the manufacturer instructions and stained with colloidal coomassie brilliant blue. Pictures were recorded directly with a Vilbert Lourmat TFX-35-M transilluminator (Marne-la-Vallée, France) under white light conditions. Fluorography of SpoIIIE-Atto647N after 12% SDS-PAGE was recorded with an Amersham Typhoon 9400 gel scanner (Amersham Biosciences, Sunnyvale, USA) using the 633 nm Helium-Neon laser.

### Preparation of DNA

For single-molecule imaging experiments, biotin-labelled λ-DNA was prepared by ligating the 12 base pairs cos overhangs of linearized λ-DNA (New England Biolabs, Ipswich, USA; at a concentration of  $8 \times 10^{-10}$  M) with 5'-biotin-modified oligo1 (5'-AGGTCGCCGCC-Biotin-3';  $8 \times 10^{-9}$  M; Eurogentec, Seraing, Belgium) using T4 DNA Ligase (New England Biolabs, Ipswich, USA).

### TIRF setup, single-molecule imaging and processing

A homemade TIRF setup based on a Zeiss Axiovert 200 inverted microscope equipped with an alpha Plan-Fluar 100×/1.45 NA objective (Zeiss, Le Peck, France) was used. The lines of a 488 nm Argon ion blue laser (Spectra physics, 163-C12, Santa Clara, USA) and a 633 nm Helium-Neon ion red laser (Melles Griot, Albuquerque, USA) were used to excite SYTOX Green (Invitrogen, France) and Atto647N fluorophores, respectively. Their fluorescence signal was collected through the same objective, passed through a filter cube containing a

dichroic mirror transmitting the 510 and 670 nm wavelengths (Chroma, Vermont, USA) and imaged onto an EM-CCD camera (Andor iXon, DU888, Belfast, Ireland). The laser power was controlled by an acoustic-optic tunable filter. The camera exposure time used was 100 ms with a gain of 300. Simultaneous imaging of DNA and SpoIIIE\* was achieved by using alternating laser excitation (28) a technology that abolishes cross-talk between emission channels.

The flow micro-fluidics chamber functionalized with biotin and Polyethylene glycol (PEG) was incubated with 0.2 mg/ml streptavidin for 10 min, and excess streptavidin washed out with TE buffer (20 mM Tris, pH 7.5, 1 mM EDTA). Biotin-labelled λ-DNA was loaded at a concentration of 1 pM into the chamber in TE buffer at a flow rate of ~50 μl/min and incubated for 15 min to allow the formation of DNA attachments through biotin-streptavidin interactions. Unbound DNA was washed out of the chamber by flowing 500 μl of a degassed buffer containing: 50 mM Tris, pH 7.5, 15 mM Dithiothreitol and 13% sucrose, at a flow velocity of 100 μl/min. For all experiments, λ-DNA was flow-stretched at a flow velocity of 100 μl/min.

For imaging λ-DNA and SpoIIIE, a modified reaction buffer (imaging buffer) was employed: 50 mM Tris (pH 7.5), 7.5 mM NaCl, 10 mM MgCl<sub>2</sub>, 15 mM Dithiothreitol, 3% Glycerol and 13% sucrose. The buffer composition was optimized for our TIRF measurements to diminish dye photobleaching and allow for longer imaging times. Photobleaching occurs when a fluorophore permanently loses the ability to fluoresce due to photon-induced chemical damage. Reactions between fluorophores and molecular oxygen permanently destroy fluorescence and yield a free radical singlet oxygen species that can chemically modify other molecules (e.g. DNA). The presence of sucrose in the imaging buffer increases the viscosity and hence decreases DNA fluctuations, while DTT serves as a scavenger of reactive oxygen species (ROS) (29). SpoIIIE ATPase activity in these conditions was comparable to activity in reaction buffer. Buffer and samples were injected into the chamber using a syringe pump (Harvard Apparatus, Holliston, USA).

### AFM imaging

Mica (Goodfellow, France) was freshly cleaved and 1 μl of a 1 mM NiCl<sub>2</sub> was deposited, incubated for 1 min and rinsed with 1 ml of deionized water (Millipore). Samples [2 nM DNA + 15 nM SpoIIIE monomer in reaction buffer without bovine serum albumin (BSA)] were then deposited and incubated for 2 min and rinsed with 3 ml of deionized water, dried with nitrogen and kept in a desiccator until imaging. AFM images were obtained with a nanoscope IIIa microscope (Veeco, France) equipped with a type-E scanner and operating in tapping mode in air using AC160 TS Olympus cantilevers as described previously (30).

Raw topographical images obtained by AFM were processed by applying a first order line-wise flattening using the nanoscope analysis software. Next, a Gaussian distribution was fitted to the experimental data (free and bound

SpoIIIE in Figure 4C) and the full width at half maximum value (FWHM) was computed to estimate the diameter of the hexamer in two perpendicular directions.

In our AFM images, DNA had a lateral size of  $\sim 11$  nm, consistent with values reported in the literature (31–33). Even with sharper tips, the resolution for DNA cannot achieve values  $< 3\text{--}5$  nm (34,35). These observations can be explained if we consider the relationship between the size of the tip and small diameter of DNA ( $\sim 2$  nm). If we consider a large tip with radius of curvature  $R$  that scans over a small sample with radius  $r$  (i.e.  $R \gg r$ ), the equation that will describe the diameter of the imaged object ( $D$ ) is represented by (36):

$$D = 4(Rr)^{0.5} \quad (1)$$

Using this equation, the image of a DNA molecule ( $r \sim 1$  nm) obtained with a tip of  $R = 10$  nm will yield  $D = 12.6$  nm, a value typically obtained in routine imaging of DNA (32).

Lateral protein sizes by AFM are affected by tip broadening. Therefore, we took into account the broadening effect of the tip in the radii of SpoIIIE complexes by using DNA as a calibration standard. We employed the geometrical approaches recently described by Winzer *et al.* for DNA as a lateral calibration standard in AFM imaging (37). We estimate the radius of the tip ( $r_{\text{Tip}}$ ) from the measured widths of the DNA sections ( $W_{\text{DNA}}$ ) by using the step-like model that results in the following approximations for the AFM tip radius:

$$r_{\text{Tip}} = \frac{(W_{\text{DNA}} - 2R_{\text{DNA}})^2}{8h_{\text{DNA}}} \quad (2)$$

From the width of the DNA sections ( $\sim 11$  nm) and height ( $h_{\text{DNA}} = 1.03$  nm; Supplementary Figure S3A) and theoretical DNA radius [ $R_{\text{DNA}} = 1$  nm, (38)] we estimate the radius of the tip to be 9.8 nm. This result is in good agreement with values reported previously for similar tips.

To estimate the radius of SpoIIIE particles ( $r_{\text{SpoIIIE}}$ ), we employed the Garcia model (39):

$$r_{\text{SpoIIIE}} \approx \frac{W_{\text{SpoIIIE}} - C_1 r_{\text{Tip}}}{C_2} \quad (3)$$

where  $W_{\text{SpoIIIE}}$  represents the total width of SpoIIIE measured from AFM ( $\sim 22$  nm), while  $C_1 = 2 - \tan\alpha - \tan\beta$ ,  $C_2 = \tan\alpha + \tan\beta + (1/\cos\alpha + 1/\cos\beta)$  and  $\alpha = \beta = 20^\circ$  were assumed using reference values from similar AFM tips. Using this equation, we estimate the radius of SpoIIIE to be 5.5 nm. This estimated radius is slightly smaller than the expected value of 6 nm, arising when taking into consideration the crystallographic structure of FtsK and our own EM results. Estimation of protein sizes from tapping mode AFM imaging in air can be affected by the degree of hydration (difficult to quantify) and often provides an underestimation of real sizes (40,41), possibly explaining the small differences between the measured and the expected SpoIIIE radius. Importantly, the radius predicted for monomeric SpoIIIE species is  $\sim 2.7$  nm, less than half the experimentally observed value. Thus, our

results are consistent with SpoIIIE existing as a single multimeric species in solution that does not change its oligomerization state upon DNA binding.

To evaluate the symmetry of SpoIIIE complexes we test statistically the differences between the mean lateral sizes of free and DNA-bound SpoIIIE in two perpendicular directions (i.e. parallel and perpendicular to DNA in DNA-bound complexes and x–y for unbound complexes), by employing the independent two-sample *t*-test analysis tool (unequal sample sizes, unequal variances) included in Origin Pro 8 (OriginLab, Northampton, U.S.A.). We assumed as null hypothesis, the equality of samples size means ( $\mu_1 - \mu_2 = 0$ ). The results of each statistical analysis are reported as:

$$t(DF) = t_{\text{value}}; P = x \quad (4)$$

where DF represents the degrees of freedom (depending on the total number of data points) estimated according to the Welch–Satterthwaite equation,  $t_{\text{value}}$  represents the statistical value obtained from the two-sample *t*-test with DF with the corresponding independent samples' means and standard deviation and  $x$  the probability  $P$  of obtaining this result simply due to chance. A small p-value (usually,  $P \leq 0.05$  or 0.01) indicates that the null hypothesis can be rejected; conversely, if the  $P$ -value obtained is larger, this indicates that the samples' means are equal with a probability  $P$ .

### Electron microscopy and image processing

Three microlitres of SpoIIIE and DNA (200 nM monomer and 50 nM, respectively, in reaction buffer without BSA or glycerol) complexes suspension were deposited onto glow-discharged, carbon-coated copper grids for 2 min. The excess solution was blotted and 4  $\mu\text{l}$  of 1% uranyl formate were applied to the grids for 1 min. The grids were then dried and observed under low-dose conditions with a JEOL 2200FS transmission electron microscope (Tokyo, Japan) operating at 200 kV. Images were recorded at a magnification of  $\times 50\,000$  using a 4k  $\times$  4k slow-scan CCD camera (Gatan, Inc. Pleasanton, USA) with defocus values ranging from 0.4 to 1.3  $\mu\text{m}$ . Single-molecule images were extracted semi-automatically from images using Boxer (42). The two-dimensional image processing was performed using IMAGIC V (43). The defocus and astigmatism values of each image were determined using CTFFIND3 (44) followed by flip of phases on each individual particle image. Normalized, band-pass filtered (150 and 20  $\text{\AA}$ ) and masked images were then auto-centered using the CENTER-IMAGE program against the average image. Some preferential views were selected by visual inspection and chosen as reference images for the multi-reference alignment program. Images were then grouped into classes and averaged according to the multi-statistical alignment procedure. The best class averages were selected visually and used as new references for new alignment cycles. The selected class averages were rotationally averaged using IMPOSE-SYMMETRY, included in the IMAGIC V software. At least three independent preparations of purified SpoIIIE were used to perform EM experiments. ‘Open’ and

'closed' particles were observed with similar frequencies in all preparations.

### Fluorescence anisotropy and ATPase activity

Binding of SpoIIIE to DNA was quantified by detection of changes in fluorescence anisotropy (FA) upon protein binding to a 43-bp, 5'-Cy3-labelled dsDNA fragment containing the sequence of interest (Eurogentec S.A., Belgium). To obtain double-stranded, fluorescently labelled DNA fragments, 200 μM solutions of Cy3-labelled oligonucleotides were annealed to its complementary oligonucleotide at equivalent concentration by brief incubation at 80° followed by slow cooling overnight at room temperature.

The sequence of DNA fragments utilized in this study for anisotropy measurements was the following:

DNA<sub>NS</sub>: 5'-GCGGAGGCCGGAGGCAGATCTTA  
CCGCTGTTGAGATCCAGC-3'

Equilibrium FA assays were performed at 27°C using a microplate reader (TECAN Safire2), exciting at 530 nm and detecting at 580 nm. SpoIIIE was added stepwise to 15 independent microplate wells containing a fixed amount of DNA-Cy3 (1.2 nM) in a total volume of 60 μl. All measurements were performed in reaction buffer.

Equilibrium binding isotherms were analysed with the following equation:

$$r = \frac{r_{\max}}{2[DNA]_T} \left\{ ([SpoIIIE]_T + [DNA]_T + K_D) - \left[ ([SpoIIIE]_T + [DNA]_T + K_D)^2 + 4[SpoIIIE]_T [DNA]_T \right]^{\frac{1}{2}} \right\} \quad (5)$$

where  $r_{\max}$  represents the maximal anisotropy change at saturating conditions,  $[DNA]_T$  and  $[SpoIIIE]_T$  are the total concentration of DNA and monomeric SpoIIIE, respectively and  $K_D$  is the apparent dissociation constant. For the fitting procedure, the dependent variable was assumed to be homoscedastic (constant variance) and the independent variable was considered to have negligible error.

ATPase measurements were performed in identical buffer and temperature conditions to those employed for anisotropy equilibrium measurements (otherwise indicated) with the addition of 3 mM ATP and reagents from EnzCheck Pyrophosphate Assay Kit (Molecular Probes, Eugene, USA). Protein concentration was in all cases 5 nM monomer.

## RESULTS

### SpoIIIE efficiently binds and translocates DNA in absence of SRS

First, we tested the ability of SpoIIIE to bind to DNA devoid of SRS and its specificity of binding, by using a single-molecule alternating laser excitation TIRF imaging approach that allowed us to image individual DNA molecules and SpoIIIE simultaneously. The SpoIIIE motor

domain was heterologously expressed, purified and N-terminal labelled with the organic dye Atto647N (hereafter SpoIIIE\*, more details in 'Materials and Methods' section). Samples of purified SpoIIIE were >90% pure and no significant degradation was observed during the labelling process (Figure 2A). We estimate the labelling efficiency of SpoIIIE\* to be 25–30% (see 'Materials and Methods' section), which translates into at least 1 to 2 fluorophores per hexameric complex. ATPase measurements of SpoIIIE\* compared with unlabelled SpoIIIE confirmed that the enzyme was completely functional with comparable specific activities (Supplementary Figure S1). Single λ-DNA molecules were introduced into a custom-made micro-fluidics chamber (8), specifically attached to a PEGylated surface and stretched by flow force (Figure 2B). Immediately after, we injected through the chamber a 1 nM hexamer solution of SpoIIIE\* in imaging buffer (see composition in 'Materials and Methods' section) at a flow velocity of 100 μl/min and incubated the samples during 5 min under no flow. At this concentration, SpoIIIE is predominantly hexamerized (27). Finally, a 5 nM solution of the DNA staining agent SYTOX Green was injected into the micro-fluidics chamber to directly visualize DNA. DNA and SpoIIIE\* were imaged by alternating laser excitation (at 488 nm and 633 nm, respectively) and fluorescence signal was detected by wide-field imaging on a sensitive emCCD camera. Representative images of DNA, SpoIIIE\* and a merge of both are shown in Figure 2C.

The acquired data was analysed to discriminate between surface-bound and DNA-bound SpoIIIE\* proteins. First, for each candidate protein, a kymograph was constructed to quantify its movement over time (Supplementary Figure S2): DNA-bound proteins will follow the slow movement of the stretched DNA tether induced by flow fluctuations (~300 nm root mean square displacement (RMSD) under our experimental conditions), while the movement of surface-bound proteins will be dramatically reduced to high-frequency, low-amplitude fluctuations (<30 nm RMSD). Second, we determined the position along the DNA tether of DNA-bound SpoIIIE\* proteins. The distribution of localizations is shown in Figure 2D. SpoIIIE\* binds λ-DNA homogeneously, thus it does not seem to bind to any obvious preferential site in λ-DNA. This, combined with the lack of SRS sequences in λ-DNA demonstrates that SpoIIIE is able to bind non-specific DNA and does not require SRS sequences to associate stably with DNA [SpoIIIE cell concentrations can reach the micromolar range at the septum (8)]. This conclusion is consistent with the low frequency of SRS in the *B. subtilis* genome (in average one SRS per 10–15 kb), as SpoIIIE would need to contact non-specific DNA thousands of times before being able to stably associate with DNA if its binding to DNA depended strictly on the presence of an SRS sequence.

Next, we performed single-molecule TIRF experiments in the presence of ATP by using the same λ-DNA substrate. SpoIIIE\* (1 nM hexamer in reaction buffer) was injected at a flow velocity of 100 μl/min through a chamber already containing single-DNA molecules attached at one end to the coverslip. Under these conditions, SpoIIIE\*

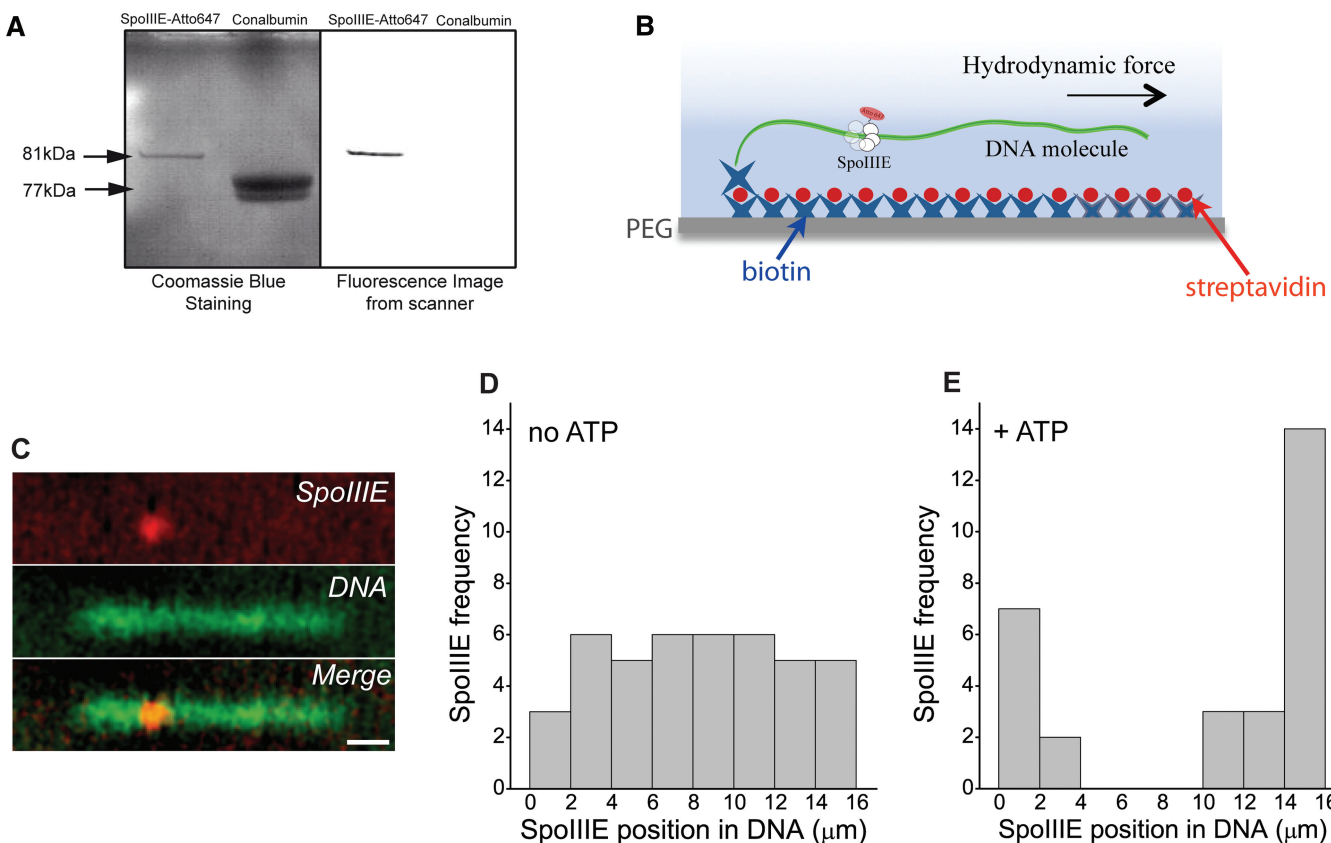


**Figure 2.** (A) SDS-PAGE analysis of purified SpoIIIE. (Left) Aliquots of purified SpoIIIE after labelling with Atto647N were taken and run on 12% SDS-PAGE. (Left) Gel stained with coomassie brilliant blue, including Conalbumin marker with relative mass in kDa. (Right) Same gel scanned with a Typhoon scanner depicting the fluorescence emission of SpoIIIE\* after excitation with 633 nm light. Aliquots contained 3  $\mu\text{g}$  of SpoIIIE per lane. (B) Experimental set-up for single-molecule TIRF imaging. Individual biotin-labelled  $\lambda$ -DNA molecules were immobilized on the PEGylated surface of the microfluidics chamber and stretched by using flow force. The position of SpoIIIE particles was determined by concomitant imaging of fluorescently labelled SpoIIIE and SYTOX-stained DNA. (C) Example of a typical field of view. (Upper and middle panel) DNA-bound SYTOX Green and SpoIIIE\* fluorescence emission. (Lower panel) Merged pseudo-coloured images of DNA and bound SpoIIIE\*. Scale bar represents 2  $\mu\text{m}$ . (D) Histograms of SpoIIIE distributions on  $\lambda$ -DNA in absence of ATP.  $N = 42$ . (E) Histograms of SpoIIIE distributions on  $\lambda$ -DNA after addition of ATP.  $N = 29$ . In panels D and E, the position of SpoIIIE particles on  $\lambda$ -DNA was measured as the minimum distance of SpoIIIE particles from the surface-bound end of DNA.

actively translocated on  $\lambda$ -DNA at velocities ( $\sim 3 \text{ kb/s}$ ) similar to those observed previously ( $4 \text{ kb/s}$ ) (3) (Supplementary Figure S2D). The position of SpoIIIE\* complexes on single  $\lambda$ -DNA molecules was determined after several minutes of incubation (equilibrium conditions). In the presence of ATP, the distribution of SpoIIIE\* changed dramatically with respect to that observed in absence of ATP, with SpoIIIE\* mainly found at the free ends of  $\lambda$ -DNA (Figure 2E, SpoIIIE position in  $\lambda$ -DNA was measured from its surface-bound end). This histogram (Figure 2E) was obtained from a different set of molecules than those used to determine the localization of SpoIIIE in the absence of ATP (Figure 2D). Overall, these results indicate that SpoIIIE translocates towards the free end by using the energy of ATP hydrolysis and that translocating motors do not preferentially dissociate when reaching the DNA free end. This latter conclusion is consistent with previously reported results and energetic considerations, as: (i) the dissociation constant of SpoIIIE from DNA is independent of the presence of ATP and (ii) the translocation off

the DNA end would entail an increased free energy due to the loss of protein- or DNA-specific contacts. Overall, these results suggest that SpoIIIE binds DNA with no sequence specificity and that activation of the motor activity of SpoIIIE does not necessarily require the presence of SRS, as recently suggested (45).

#### Influence of nucleotide in the binding of SpoIIIE to DNA

ATP-driven conformational changes of the RecA-like domains in ASCE (Additional Strand Catalytic E) fold family proteins have been shown to be responsible for the translocation of nucleic acids by the repositioning of nucleic acid binding sites on the protein surface (46). These conformational changes can be reflected by modifications in the binding affinity of SpoIIIE in the presence of different nucleotides or mutants preventing nucleotide binding/hydrolysis. We previously showed that SpoIIIE binds efficiently to non-specific DNA (43-bp DNA fragment with no SRS, hereafter DNA<sub>NS</sub>, see ‘Materials and Methods’ section), with the binding isotherm well described by a simple single-site model [Equation (4),

$K_D = 60 \pm 5 \text{ nM}$ ; (27)]. This length of DNA is sufficient to stimulate the ATPase activity of SpoIIIE (Supplementary Figure S3A). To further investigate the role of ATP in the binding mechanism of SpoIIIE, we used a fluorescence anisotropy-based assay that directly measures the binding of SpoIIIE to DNA. The binding of large proteins, such as SpoIIIE, to short fluorescently labelled DNA fragments decreases the rotational diffusion of the DNA molecule and increases the fluorescence anisotropy of the attached fluorophore (Figure 3A) (47). This signal was used to determine the total bound fraction as a function of protein concentration in the presence of ATP, ADP, a non-hydrolysable analogue of ATP and for an ATPase-deficient mutant (48).

First, we tested whether SpoIIIE binding was affected by the presence of ATP or the ability of SpoIIIE to bind nucleotide. For the HerA/FtsK family of DNA translocases to which SpoIIIE belongs, ATP-binding sites are situated at the interface of adjacent protomers (46), thus ATP binding could play a role in subunit coordination that may be reflected by modifications in the affinity of SpoIIIE for DNA. When we evaluate the effect of saturating ATP (3 mM) in the binding of SpoIIIE, we observe that the affinity of SpoIIIE for DNA<sub>NS</sub> is not altered (Figure 3B;  $K_{D,ATP} = 61 \pm 11 \text{ nM}$ ). Additionally, no modifications of the binding mode are observed. Small conformational changes may be translated into modifications of the total number of contacts present between SpoIIIE and DNA and thus into affinity changes. As no significant alteration of binding affinity are observed, this suggests that ATP binding does not promote a detectable conformational change.

Next, we tested whether the ATP-binding capacity of the motor, even in absence of nucleotide, affects its ability to efficiently bind DNA. To this aim, we employed a SpoIIIE variant with a mutation in the Walker A ATP-binding site (G467S, hereafter SpoIIIE<sup>467</sup>). Previous studies showed that mutations in the equivalent residue in P-loop Walker ATP/GTPases abolish nucleotide binding (49), and that strains of *B. subtilis* carrying this mutation are severely defective in chromosome translocation during sporulation (48). Our results show that SpoIIIE<sup>467</sup> binds DNA with an affinity ( $K_{D, \text{SpoIIIE}^{467}} = 63 \pm 3 \text{ nM}$ ) similar to that of wild-type SpoIIIE (Figure 3C). Overall, these results indicate that ATP binding does not play a significant role in DNA binding by SpoIIIE, and would be consistent with ATP binding not being involved in hexamerization.

However, given the fast hydrolysis rate of ATP by SpoIIIE, ATP-bound states could be short-lived and the existence of intermediate, conformationally distinguishable states may have been undetectable by our previous experiments. To investigate whether DNA–protein contacts are affected during the ATP cycle, we performed experiments in the presence of 3 mM ATPγS. SpoIIIE is able to hydrolyse this ATP analogue at a lower rate than ATP (~2.5 times more slowly, Supplementary Figure S3B), suggesting that SpoIIIE is able to bind it efficiently. Interestingly, the affinity of SpoIIIE for DNA does not change in presence of ATPγS (Figure 3B,  $K_D, \text{ATP}\gamma\text{S} = 60 \pm 9 \text{ nM}$ ). Considering that at the saturating

concentrations of ATP and ATPγS employed in our experiments, most of SpoIIIE will bind to nucleotides before encountering DNA, these results suggest that the DNA-bound SpoIIIE-ATP conformation is not more stably bound to DNA than that of the nucleotide-free protein and that conformational changes in the motor domain taking place before ATP hydrolysis do not significantly affect the DNA–protein interface.

For DNA motors, major conformational changes in the protein allow conversion of chemical energy from ATP hydrolysis into mechanical movement (50). To test this hypothesis for SpoIIIE, we measured the DNA-binding affinity of SpoIIIE after ATP hydrolysis by performing experiments in the presence of saturating amounts of ADP (3 mM). In this case, we observed a noticeable increase in affinity (Figure 3B;  $K_{D,ADP} = 43 \pm 9 \text{ nM}$ ), suggesting a small conformational change after hydrolysis of ATP during translocation ( $\Delta\Delta G \sim -0.8 \text{ kJ/mol}$ ). Interestingly, the affinity of SpoIIIE for DNA is unchanged in the presence of the slowly hydrolysable ATP analogue. Thus, the release of inorganic phosphate, but not of ADP, during the ATP hydrolysis cycle may be responsible for the power stroke. Further structural studies are necessary to confirm or refute this hypothesis and to determine the exact mechanism by which ATP-induced conformational changes are converted into DNA movement. In all cases, binding curves showed no cooperativity, suggesting a purely bi-molecular interaction with no intermediates. Cooperativity in multi-subunit enzymes can be observed if the strength of interaction between subunits is coupled to ligand binding (51,52). Thus, occurrence of sigmoidicity in the binding isotherm should be observed if the oligomer is largely dissociated at protein concentrations where DNA binding occurs. In other words, binding cooperativity depends on whether the oligomerization constant exceeds the DNA-binding equilibrium constant (53). The absence of sigmoidicity in our binding curves is thus in good agreement with previous results which indicate that the oligomerization constant of SpoIIIE is independent of the presence of DNA and ~15 times smaller [ $K_{\text{Olig}} \sim 4 \text{ nM}$ , (27)] than the dissociation constants reported here. The absence of cooperativity suggests that there are no major conformational changes in SpoIIIE upon binding to DNA even in the presence of nucleotides; neither monomer–monomer interactions that would facilitate the formation of an active hexamer upon binding of a first subunit to DNA [as proposed by the preferential loading model, (14)]. Overall, the successful description of our binding isotherms by a single-site binding model [Equation (5), ‘Materials and Methods’ section] suggest that the binding mechanism does not involve several steps and is consistent with a process involving the binding of pre-assembled hexamers rather than the oligomerization of monomers on DNA.

#### SpoIIIE does not thread through a DNA end but directly binds dsDNA

The results presented previously suggest that SpoIIIE binds DNA non-specifically as a pre-formed hexamer

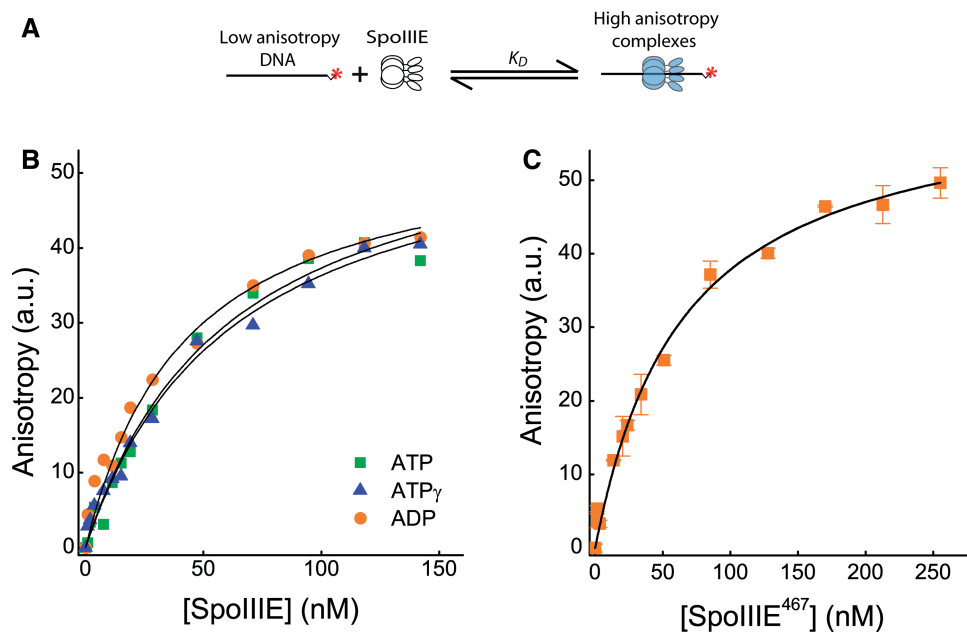


**Figure 3.** (A) Scheme illustrating the set up for SpoIIIE–DNA binding experiments monitored by fluorescence anisotropy. Black solid line represents dsDNA, red asterisk the cy3 fluorophore and hexamer represents unbound (white) or DNA-bound (blue) SpoIIIE. (B) SpoIIIE–DNA equilibrium binding isotherms in the presence of nucleotide and analogues. Addition of ATP (green squares) and non-hydrolyzable ATP ( $\text{ATP}\gamma$ , blue triangles) did not affect the binding mechanism of wild-type SpoIIIE nor its affinity for DNA suggesting a conformational change after ATP hydrolysis. (C) DNA equilibrium binding isotherm of an ATP-binding-deficient mutant (SpoIIIE $^{467}$ ). SpoIIIE $^{467}$  binds DNA with similar affinity to wild-type SpoIIIE, in agreement with previous results suggesting that ATP has no role in SpoIIIE binding to DNA. Concentration of SpoIIIE and SpoIIIE $^{467}$  in the x-axis is expressed as monomer. Solid lines in B and C represent the fitting of Equation (4) (see ‘Materials and Methods’ section) to the experimental dataset, with the best fitting parameters  $K_{D,\text{ATP}} = 61 \pm 11 \text{ nM}$ ,  $K_{D,\text{ATP}\gamma} = 60 \pm 9 \text{ nM}$  and  $K_{D,\text{ADP}} = 43 \pm 9 \text{ nM}$  and  $K_{D,\text{SpoIIIE}^{467}} = 63 \pm 3 \text{ nM}$ . Error bars for each data point in the three conditions in panel B were removed for the clarity of the figure. Relative errors of each data point were in all cases <10%.

and moves to DNA ends after addition of nucleotide. To directly visualize whether SpoIIIE needs a free DNA end to bind and whether oligomerization state depends on DNA binding, we turned to the study of SpoIIIE in absence and presence of DNA by AFM using closed DNA molecules. Circular closed plasmid DNA substrates (3 kb in length) were incubated with SpoIIIE at a 2:1 hexamer:DNA ratio ([DNA] = 2 nM) without ATP for 15 min before deposition onto a mica surface and drying under  $\text{N}_2$  flow. Typical images of DNA alone, DNA-bound and free SpoIIIE particles are shown in Figure 4A and B and Supplementary Figure S4A–C. The observed width of DNA (~11 nm, Figure 4C) is in good agreement with typical DNA sizes by AFM (32,33,36). The distribution of SpoIIIE bound to DNA was homogeneous and the number of proteins bound per plasmid was in good agreement with concentration ratios (~1–2 hexamers per plasmid in Figure 4A and B; higher ratios in Supplementary Figure S4B and C), suggesting that the observed species represent SpoIIIE hexamers. The hexameric crystallographic structure of *Pseudomonas aeruginosa* FtsK (PaFtsK) shows that hexamers possess a central channel that can accommodate dsDNA and indirect measurements using EM of FtsK bound to DNA fragments of different lengths strongly suggest that DNA passes through the central hole of the FtsK ring (21). Height measurements of DNA (mean  $\pm$  sd =  $1.1 \pm 0.1 \text{ nm}$ , Figure 4C and Supplementary Figure S3A), free SpoIIIE ( $2.6 \pm 0.4 \text{ nm}$ ;

Figure 4C and Supplementary Figure S3B) and DNA-bound SpoIIIE complexes ( $2.8 \pm 0.2 \text{ nm}$ ; Figure 4C and Supplementary Figure S3C) are consistent with DNA threading though the putative central pore in SpoIIIE. More importantly, these data clearly demonstrate that SpoIIIE can bind efficiently to circular DNA, indicating that binding of SpoIIIE to DNA does not involve threading through a DNA end. In addition to our TIRF imaging results (Figure 2E), triplex displacement assays using the same substrate used for AFM measurements (but linearized) confirmed that SpoIIIE is able to efficiently translocate on DNA, reach DNA ends and displace the triplex in an ATP-dependent manner (3), consistent with the DNA-bound complexes observed by AFM being translocation proficient.

Next, we quantified the lateral size of DNA-bound and free SpoIIIE complexes by calculating the FWHM from a Gaussian fitting to the height profiles (Figure 4C) in two directions (parallel and perpendicular to DNA in DNA-bound complexes and x-y for unbound complexes). The size of a protein in tapping mode AFM is affected by tip broadening and even when this effect is taken into account, measurements of protein sizes can be affected by hydration and usually tend to underestimate protein volumes (40,41) (see discussion in the ‘Materials and Methods’ section). Despite these effects, lateral size distributions can be used to compare different DNA-bound states and evaluate the presence of different oligomeric species. Lateral sizes are compatible with SpoIIIE

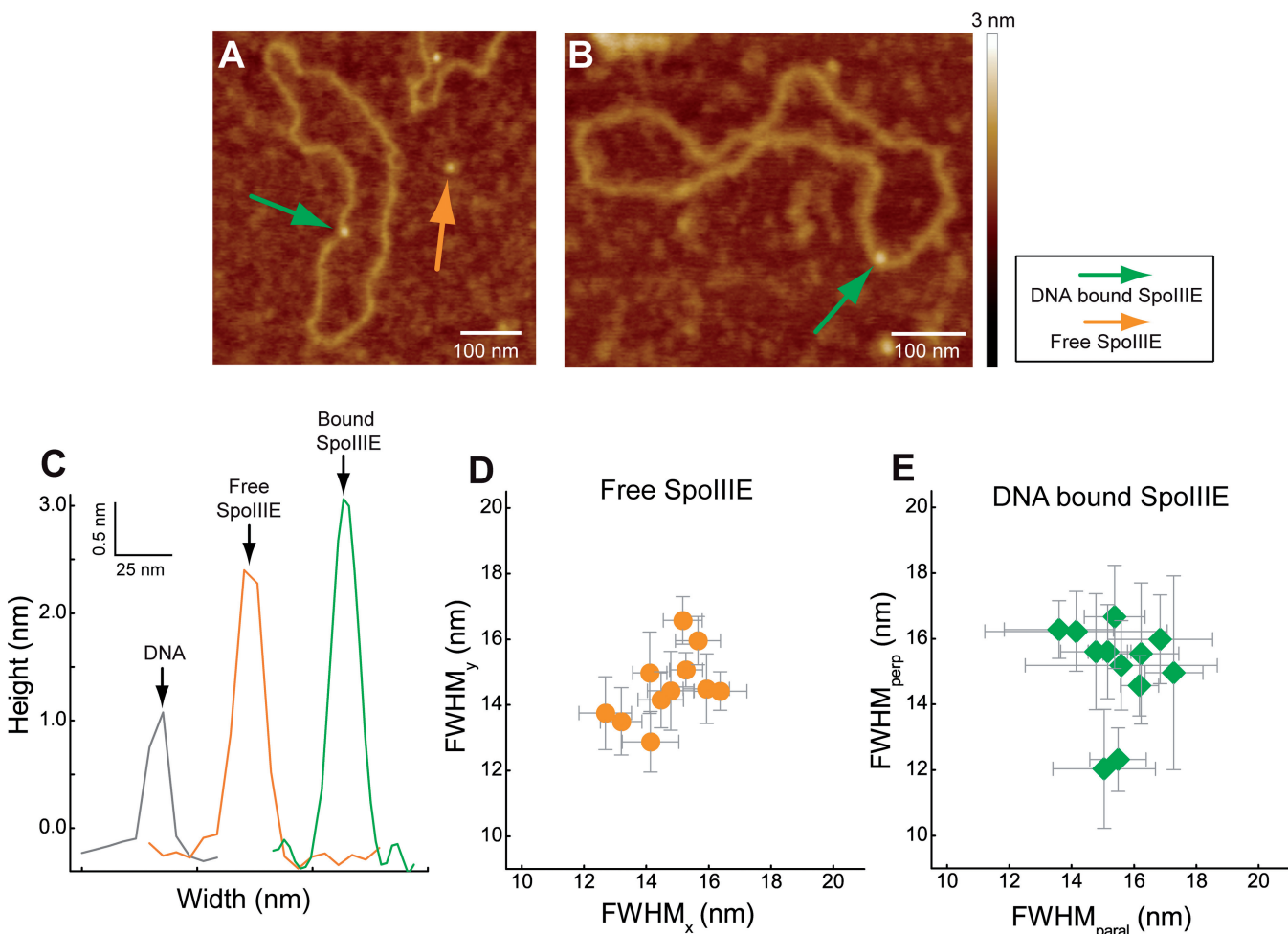


**Figure 4.** (A), (B) AFM imaging of SpoIIIE–DNA complexes on circular DNA. Orange arrow indicates free SpoIIIE and green arrows indicate SpoIIIE bound to DNA. (C) Cross-section values of height and length of a representative DNA (grey line), free SpoIIIE (orange solid line) and DNA-bound SpoIIIE complexes (green solid line). (D), (E) Lateral distribution of sizes of free and DNA-bound SpoIIIE complexes in two directions. A Gaussian distribution was fitted to the experimental height data measured in the two normal directions (parallel and perpendicular to DNA in DNA-bound complexes and x-y for unbound complexes) and the FWHM of the height profile was computed to estimate the diameter of free and DNA-bound hexamers. The mean FWHM (in x and y directions) were (nm):  $14.70 \pm 1.13$  and  $14.56 \pm 1.06$  for free SpoIIIE particles and  $15.47 \pm 1.05$  and  $15.08 \pm 1.47$  for DNA-bound SpoIIIE. Mean FWHM (in both directions combined) were (nm):  $14.63 \pm 1.07$  nm for free SpoIIIE and  $15.27 \pm 1.27$  for DNA-bound particles. These reported values were employed to test statistically the differences between the mean lateral sizes of free and DNA-bound SpoIIIE described in the main text [Equation (4), ‘Material and Methods’ section].

assembling as a multimeric rather than monomeric species (see discussion in ‘Materials and Methods’ section). In addition, SpoIIIE complexes are symmetric [ $t(20) = 0.29$ ,  $P \geq 0.76$  for free and  $t(21) = 0.75$ ,  $P \geq 0.46$  for DNA-bound complexes, using the independent two-sample *t*-test analysis, see ‘Materials and Methods’ section] and the distribution of protein sizes seems homogeneous. Although these data do not allow us to completely discard the existence of a small degree of oligomeric heterogeneity, fluorescence correlation spectroscopy experiments (27) and EM imaging confirm that these species represent SpoIIIE hexamers (see below). Importantly, the average size of SpoIIIE complexes does not depend on DNA-bound state [ $t(43) = 1.84$ ,  $P \geq 0.07$ ], consistent with pre-formed hexamers being the species that binds dsDNA.

Overall, these results suggest that pre-formed complexes bind DNA directly from solution in a single step, at

concentrations considerably lower (<15 nM monomer) than the affinity of SpoIIIE for non-specific DNA ( $K_D = 60 \pm 5$  nM) with no sequence specificity. These findings are in agreement with a recent study showing that SpoIIIE exists in a monomeric form at low concentrations (<1 nM monomer) and predominantly in hexameric form at high concentrations (>6 nM monomer) independently of the presence of DNA (27). Taken together, these results are in strong contradiction with the preferential loading model by which FtsK/SpoIIIE hexamers oligomerize specifically on KOPS/SRS (14,26).

#### SpoIIIE hexamers display open and closed conformations in solution

Our AFM results showing that SpoIIIE can directly bind closed circular DNA molecules raise several questions: how can a closed hexamer bind a circular dsDNA

molecule? Can SpoIIIE hexamers break open to bind DNA and then close to translocate? Due to the intrinsic lateral resolution limits in our AFM experiments, we addressed these questions by EM. SpoIIIE/DNA complexes were negatively stained using uranyl-formate and observed by EM. (Figure 5A). In the presence of an excess of 43 bp DNA ( $[DNA] = 50 \text{ nM}$ ), SpoIIIE mainly assembled in uniform, ring-like particles as showed by black arrows in Figure 5A. However, open-ring-like particles (dotted squares on Figure 5A) were also visualized at a lower frequency (28%). These two different conformations that will be now referred to as closed and open states are certainly directly visible from raw EM images of isolated particles (Figure 5B), and were observed with different SpoIIIE preparations. We also observed side-view of these particles, but these were often more difficult to detect than front-view particles due to their lack of symmetry (orange arrows in Figure 5A). A majority of open-ring particles were observed in the absence of DNA (Supplementary Figure S6), consistent with the closure of SpoIIIE on DNA decreasing its dissociation rate.

Open- and closed-ring-like particles show an outer diameter of  $\sim 10 \text{ nm}$  and a large inner hole of  $\sim 2.5 \text{ nm}$  (Figure 5B), consistent with our estimates from AFM imaging and slightly smaller than the hexameric EM and crystallographic structure of *P. aeruginosa* FtsK (PaFtsK) (21) and with our estimates from AFM imaging. No detectable monomer or other intermediate species were present, in agreement with our AFM and binding studies and ruling out models in which individual monomers bind sequentially to DNA to form a hexamer (14). With 43-bp DNA fragments, we observed well-defined face-on hexameric rings (Figure 5C, left panel). This hexameric organization of SpoIIIE is clearer from class averages (Figure 5C, right panel), where six protruding extremities are visible. This is confirmed when inspecting their corresponding C6 symmetry imposed images in which the hexameric organization is conserved. Unlike PaFtsK, in solution SpoIIIE mainly assembles as a single hexamer rather than a head-to-head double hexamer (21).

The shape non-homogeneity of open-ring particles clearly indicates a structural heterogeneity of SpoIIIE complexes, as observed for other ring-shaped molecular motors [e.g. the transcription terminator factor  $\rho$ , (54)]. Solely from our EM imaging, we cannot completely rule out the possibility that these particles represent incomplete hexamers. However, other evidence strongly suggests that open-ring particles represent out-of-plane hexamers: (i) SpoIIIE undergoes a cooperative oligomerization from monomer to hexamer at  $\sim 4 \text{ nM}$  (27). Therefore, at the concentrations used for EM experiments ( $\sim 200 \text{ nM}$  monomer), SpoIIIE is completely hexamerized; (ii) alternative oligomeric species (monomers or dimers) are not observed by AFM or EM imaging (Figures 4–5). Open-ring particles are reminiscent of the ‘lock-washer’ conformation adopted by the hexameric  $\rho$  helicase, a split-open ring in which subunits follow a helical staircase (instead of a planar closed ring) with an opening between subunits of  $\sim 1.2 \text{ nm}$ , large enough to accommodate single-stranded RNA (55). Similarly, open-ring-like

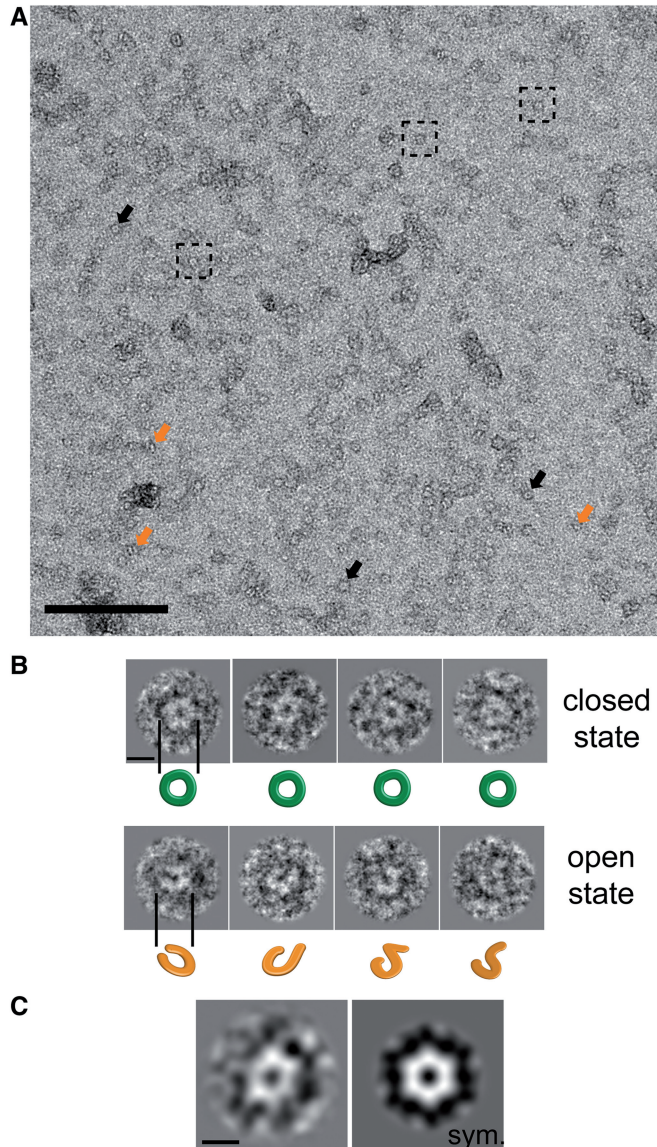


**Figure 5.** (A) EM of negatively stained SpoIIIE in presence of DNA. Black arrows and dotted squares indicate closed and open states, respectively. Orange arrows indicate side-view of SpoIIIE particles. Scale bar, 100 nm. (B) Raw particle images illustrate closed- and open-ring-like conformations. Proteins are in white. Schematic drawings of particles in closed (green) and open state (orange) images are presented below for clarity. Scale bar, 5 nm. (C) Representative class average of the closed state corresponding to the average of 37 individual particle images and their corresponding C6 symmetry imposed images (noted sym.) revealing the hexameric organization of SpoIIIE. The SpoIIIE hexameric ring displays an outer diameter of  $\sim 100 \text{ \AA}$  with a central channel of  $\sim 25 \text{ \AA}$ . Scale bar, 5 nm.

SpoIIIE particles are compatible with a helical open-ring structure and contain a large opening of  $\sim 2.5 \pm 1 \text{ nm}$ , large enough to accommodate dsDNA. Overall, these results suggest that the mechanism of SpoIIIE binding to dsDNA involves threading of dsDNA between neighbouring monomers of an open-ring SpoIIIE hexamer and closure of the ring may lead to the formation of a translocation-competent structure. Based on our binding data, we believe these conformational changes are not likely to

be affected by ATP binding or hydrolysis, although they may be favoured by the binding of SpoIIIIE- $\gamma$  domains to SRS, the sequences regulating motor directionality.

## DISCUSSION

In this article, we investigated the mechanism of DNA binding by SpoIIIIE by using a combination of single-molecule, biochemical and structural methods. First, our TIRF imaging and ensemble binding studies unambiguously show that SpoIIIIE is able to associate to non-specific DNA with high affinity and no specificity. In addition, our data are consistent with SpoIIIIE binding being unaffected by ATP binding or hydrolysis. Second, AFM imaging of SpoIIIIE-DNA complexes show that SpoIIIIE is able to bind dsDNA without requiring a free DNA end and is consistent with free and DNA-bound SpoIIIIE existing as pre-formed single hexamers. Finally, we used electron microscopy to reveal the existence of open and closed SpoIIIIE hexameric structures in solution that provide a rationale for how pre-formed SpoIIIIE hexamers may be able to bind closed circular DNA molecules. These results are in contrast to the solution behaviour of PaFtsK, a protein that forms single hexamers at high concentrations ( $>10\ \mu\text{M}$  monomer) in the absence and presence of short dsDNA fragments, but double hexamers in longer dsDNAs (21). These differences in solution oligomerization behaviour may be due to the protein construct used, which in the case of SpoIIIIE included the full unstructured linker joining the motor and membrane domains (SpoIIIIEL). Interestingly, the first 29 amino acids of SpoIIIIEL are predicted to fold as an  $\alpha$ -helix and may participate in the process of hexamerization.

*In vivo*, SpoIIIIE is recruited to the sporulation septum where it is responsible for the processive, independent translocation of the two chromosomal arms in an independent fashion (3,8,10,56). SpoIIIIE hexamerizes at nanomolar concentrations [ $K_{\text{olig}} \sim 4\text{nM}$  monomer, (27)], yet its local concentration at the site of DNA translocation can reach the micromolar level (8,56). Thus, SpoIIIIE is expected to be fully hexamerized when it first encounters DNA at the end of septal closure (8). This raises the question of how do closed hexamers bind the two arms of a topologically closed circular chromosome. Our finding that SpoIIIIE hexamers show closed and open conformations in solution provides a simple mechanism for SpoIIIIE to bind DNA without hexamer disassembly.

The ensemble of the results presented in this article is inconsistent with models predicting oligomerization of FtsK/SpoIIIIE on KOPS/SRS (14,26). Our current and previous results (27) also rule out models proposing the direct and specific binding of pre-formed hexamers to KOPS/SRS (25). Previously, it was shown that: (i) SpoIIIIE is able to bind dsDNA as a pre-formed hexamer that is able to diffuse/hop on DNA to find its target SRS sequence despite the low density of SRS in DNA [approximately one instance per 10 kb (3)] (27). This search process is efficient despite the low specificity for SRS and importantly, does not require the energy of

ATP hydrolysis (27); (ii) the SpoIIIIE motor activity is stimulated upon encountering a permissive SRS sequence. This activation requires specific interactions between SpoIIIIE- $\gamma$  and SRS as well as oligomerization of SpoIIIIE- $\gamma$  (27,45); (iii) importantly, a recent study showed that SpoIIIIE- $\gamma$  inhibits the ATPase activity of SpoIIIIE in the absence of DNA or SRS and considerably enhances this activity when SpoIIIIE binds SRS in the permissive direction (45).

The results presented in this article strongly suggest that the existence of two structural forms of SpoIIIIE could be related to the conversion between translocation inactive and active forms. Thus, open-ring inactive hexamers could associate to non-specific DNA and search for the SRS sequence without using the energy of ATP hydrolysis. Ensuing orientation-specific SRS/SpoIIIIE- $\gamma$  interactions and SpoIIIIE- $\gamma$  oligomerization could thus lead to conformational changes in the motor that trigger its conversion into a closed, active form that is able to pump the chromosome by ATP-fuelled DNA translocation. These conformational transitions between open/inactive and closed/active forms can occur in absence of SRS (as SpoIIIIE does not require SRS for ATP-fuelled translocation); however, they may be regulated by SpoIIIIE- $\gamma$  (27,45). This mechanism justifies the need for the presence of SRS sequences scattered along the entire chromosome to permit the re-start of directional DNA translocation after motor dissociation induced by DNA blockages (57) or spontaneous dissociation due to the finite processivity of the motor (3).

## SUPPLEMENTARY DATA

Supplementary Data are available at NAR Online.

## ACKNOWLEDGEMENTS

Fluorescence anisotropy and TIRF experiments were performed at the Biophysics facility of the Centre de Biochimie Structurale (CBS) funded by the Plate-forme Intégrée de Biologie Structurale (IBISA) and France BioImaging. We thank Emmanuel Margeat and Martin Cohen-Gonsaud for critical reading and discussions of the manuscript. D.I.C., S.T. and M.N. conceived and designed the experiments. D.I.C., S.T., C.G., P.E.M., J. L.-K.-H. and P.B. performed the experiments. D.I.C., S.T., A.L.G., P.B., P.E.M. and M.N. analysed the data. D.I.C. and M.N. wrote the article.

## FUNDING

The Human Frontiers Science Program [Career Development Award 00017/2009 to M.N.]; the Institut National de la Santé et la Recherche Médicale (to M.N.); the European Research Council [Starting Grant 260787 to M.N.]. Funding for open access charge: Human Frontiers Science Program.

*Conflict of interest statement.* None declared.

## REFERENCES

- Saleh,O.A., Perals,C., Barre,F.X. and Allemand,J.F. (2004) Fast, DNA-sequence independent translocation by FtsK in a single-molecule experiment. *EMBO J.*, **23**, 2430–2439.
- Pease,P.J., Levy,O., Cost,G.J., Gore,J., Ptacin,J.L., Sherratt,D., Bustamante,C. and Cozzarelli,N.R. (2005) Sequence-directed DNA translocation by purified FtsK. *Science*, **307**, 586–590.
- Ptacin,J.L., Nollmann,M., Becker,E.C., Cozzarelli,N.R., Pogliano,K. and Bustamante,C. (2008) Sequence-directed DNA export guides chromosome translocation during sporulation in *Bacillus subtilis*. *Nat. Struct. Mol. Biol.*, **15**, 485–493.
- Lee,J.Y., Finkelstein,I.J., Crozat,E., Sherratt,D.J. and Greene,E.C. (2012) Single-molecule imaging of DNA curtains reveals mechanisms of KOPS sequence targeting by the DNA translocase FtsK. *Proc. Natl Acad. Sci. USA*, **109**, 6531–6536.
- Ben-Yehuda,S., Rudner,D.Z. and Losick,R. (2003) RacA, a bacterial protein that anchors chromosomes to the cell poles. *Science*, **299**, 532–536.
- Errington,J. (2003) Regulation of endospore formation in *Bacillus subtilis*. *Nat. Rev. Microbiol.*, **1**, 117–126.
- Errington,J., Murray,H. and Wu,L.J. (2005) Diversity and redundancy in bacterial chromosome segregation mechanisms. *Philos. Trans. R Soc. Lond. B Biol. Sci.*, **360**, 497–505.
- Fiche,J.B., Cattoni,D.I., Diekmann,N., Langerak,J.M., Clerc,C., Royer,C.A., Margeat,E., Doan,T. and Nollmann,M. (2013) Recruitment, Assembly, and Molecular Architecture of the SpoIIIE DNA Pump Revealed by Superresolution Microscopy. *PLoS Biol.*, **11**, e1001557.
- Wu,L.J. and Errington,J. (1997) Septal localization of the SpoIIIE chromosome partitioning protein in *Bacillus subtilis*. *EMBO J.*, **16**, 2161–2169.
- Sharp,M.D. and Pogliano,K. (2002) Role of cell-specific SpoIIIE assembly in polarity of DNA transfer. *Science*, **295**, 137–139.
- Ben-Yehuda,S., Rudner,D.Z. and Losick,R. (2003) Assembly of the SpoIIIE DNA translocase depends on chromosome trapping in *Bacillus subtilis*. *Curr. Biol.*, **13**, 2196–2200.
- Bath,J., Wu,L.J., Errington,J. and Wang,J.C. (2000) Role of *Bacillus subtilis* SpoIIIE in DNA transport across the mother cell-prespore division septum. *Science*, **290**, 995–997.
- Barre,F.X. (2007) FtsK and SpoIIIE: the tale of the conserved tails. *Mol. Microbiol.*, **66**, 1051–1055.
- Graham,J.E., Sherratt,D.J. and Szczelkun,M.D. (2010) Sequence-specific assembly of FtsK hexamers establishes directional translocation on DNA. *Proc. Natl Acad. Sci. USA*, **107**, 20263–20268.
- Wang,L. and Lutkenhaus,J. (1998) FtsK is an essential cell division protein that is localized to the septum and induced as part of the SOS response. *Mol. Microbiol.*, **29**, 731–740.
- Yu,X.C., Tran,A.H., Sun,Q. and Margolin,W. (1998) Localization of cell division protein FtsK to the *Escherichia coli* septum and identification of a potential N-terminal targeting domain. *J. Bacteriol.*, **180**, 1296–1304.
- Liu,N.J., Dutton,R.J. and Pogliano,K. (2006) Evidence that the SpoIIIE DNA translocase participates in membrane fusion during cytokinesis and engulfment. *Mol. Microbiol.*, **59**, 1097–1113.
- Fleming,T.C., Shin,J.Y., Lee,S.H., Becker,E., Huang,K.C., Bustamante,C. and Pogliano,K. (2010) Dynamic SpoIIIE assembly mediates septal membrane fission during *Bacillus subtilis* sporulation. *Genes Dev.*, **24**, 1160–1172.
- Dubarry,N., Possoz,C. and Barre,F.-X. (2010) Multiple regions along the *Escherichia coli* FtsK protein are implicated in cell division. *Mol. Microbiol.*, **78**, 1088–1100.
- Lesterlin,C., Pages,C., Dubarry,N., Dasgupta,S. and Cornet,F. (2008) Asymmetry of chromosome Replichores renders the DNA translocase activity of FtsK essential for cell division and cell shape maintenance in *Escherichia coli*. *PLoS Genet.*, **4**, e1000288.
- Massey,T.H., Mercogliano,C.P., Yates,J., Sherratt,D.J. and Lowe,J. (2006) Double-stranded DNA translocation: structure and mechanism of hexameric FtsK. *Mol. Cell*, **23**, 457–469.
- Aussel,L., Barre,F.X., Aroyo,M., Stasiak,A., Stasiak,A.Z. and Sherratt,D. (2002) FtsK Is a DNA motor protein that activates chromosome dimer resolution by switching the catalytic state of the XerC and XerD recombinases. *Cell*, **108**, 195–205.
- Levy,O., Ptacin,J.L., Pease,P.J., Gore,J., Eisen,M.B., Bustamante,C. and Cozzarelli,N.R. (2005) Identification of oligonucleotide sequences that direct the movement of the *Escherichia coli* FtsK translocase. *Proc. Natl Acad. Sci. USA*, **102**, 17618–17623.
- Bigot,S., Saleh,O.A., Lesterlin,C., Pages,C., El Karoui,M., Dennis,C., Grigoriev,M., Allemand,J.F., Barre,F.X. and Cornet,F. (2005) KOPS: DNA motifs that control *E. coli* chromosome segregation by orienting the FtsK translocase. *EMBO J.*, **24**, 3770–3780.
- Bigot,S., Saleh,O.A., Cornet,F., Allemand,J.F. and Barre,F.X. (2006) Oriented loading of FtsK on KOPS. *Nat. Struct. Mol. Biol.*, **13**, 1026–1028.
- Lowe,J., Ellonen,A., Allen,M.D., Atkinson,C., Sherratt,D.J. and Grainge,I. (2008) Molecular mechanism of sequence-directed DNA loading and translocation by FtsK. *Mol. Cell*, **31**, 498–509.
- Cattion,D.I., Chara,O., Godefroy,C., Margeat,E., Trigueros,S., Milhiet,P.E. and Nollmann,M. (2013) SpoIIIE mechanism of directional translocation involves target search coupled to sequence-dependent motor stimulation. *EMBO Rep.*, **14**, 473–479.
- Kapanidis,A.N., Laurence,T.A., Lee,N.K., Margeat,E., Kong,X. and Weiss,S. (2005) Alternating-laser excitation of single molecules. *Acc. Chem. Res.*, **38**, 523–533.
- Zeller,A., Wenzl,M.V., Beretta,M., Stessel,H., Russwurm,M., Koesling,D., Schmidt,K. and Mayer,B. (2009) Mechanisms underlying activation of soluble guanylate cyclase by the nitroxyl donor Angel's salt. *Mol. Pharmacol.*, **76**, 1115–1122.
- Milhiet,P.E., Yamamoto,D., Berthoumieu,O., Dosset,P., Le Grimellec,C., Verdier,J.M., Marchal,S. and Ando,T. (2010) Deciphering the structure, growth and assembly of amyloid-like fibrils using high-speed atomic force microscopy. *PLoS One*, **5**, e13240.
- Lyubchenko,Y., Shlyakhtenko,L., Harrington,R., Oden,P. and Lindsay,S. (1993) Atomic force microscopy of long DNA: imaging in air and under water. *Proc. Natl Acad. Sci. USA*, **90**, 2137–2140.
- Lyubchenko,Y.L. (2011) Preparation of DNA and nucleoprotein samples for AFM imaging. *Micron*, **42**, 196–206.
- Bustamante,C., Keller,D. and Yang,G. (1993) Scanning force microscopy of nucleic acids and nucleoprotein assemblies. *Curr. Opin. Struct. Biol.*, **3**, 363–372.
- Chen,L., Cheung,C.L., Ashby,P.D. and Lieber,C.M. (2004) Single-walled carbon nanotube AFM probes: optimal imaging resolution of nanoclusters and biomolecules in ambient and fluid environments. *Nano Lett.*, **4**, 1725–1731.
- Klinov,D., Dwir,B., Kapon,E., Borovok,N., Molotsky,T. and Kotlyar,A. (2007) High-resolution atomic force microscopy of duplex and triplex DNA molecules. *Nanotechnology*, **18**, 225102.
- Bustamante,C., Vesenka,J., Tang,C.L., Rees,W., Guthold,M. and Keller,R. (1992) Circular DNA molecules imaged in air by scanning force microscopy. *Biochemistry*, **31**, 22–26.
- Winzer,A.T., Kraft,C., Bhushan,S., Stepanenko,V. and Tessmer,I. (2012) Correcting for AFM tip induced topography convolutions in protein-DNA samples. *Ultramicroscopy*, **121**, 8–15.
- Watson,J.D. and Crick,F.H.C. (1953) The Structure of DNA. *Cold Spring Harb. Symp. Quant. Biol.*, **18**, 123–131.
- Garcia,V.J., Martinez,L., Briceno-Valero,J.M. and Schilling,C.H. (1997) Dimensional metrology of nanometric spherical particles using AFM: I, model development. *Probe Micr.*, **1**, 107–116.
- Wyman,C., Rombel,I., North,A.K., Bustamante,C. and Kustu,S. (1997) Unusual oligomerization required for activity of NtrC, a bacterial enhancer-binding protein. *Science*, **275**, 1658–1661.
- Bustamante,C. and Rivetti,C. (1996) Visualizing protein-nucleic acid interactions on a large scale with the scanning force microscope. *Annu. Rev. Biophys. Biomol. Struct.*, **25**, 395–429.
- Ludtke,S.J., Baldwin,P.R. and Chiu,W. (1999) EMAN: semiautomated software for high-resolution single-particle reconstructions. *J. Struct. Biol.*, **128**, 82–97.
- van Heel,M., Harauz,G., Orlova,E.V., Schmidt,R. and Schatz,M. (1996) A new generation of the IMAGIC image processing system. *J. Struct. Biol.*, **116**, 17–24.
- Mindell,J.A. and Grigorieff,N. (2003) Accurate determination of local defocus and specimen tilt in electron microscopy. *J. Struct. Biol.*, **142**, 334–347.

45. Besprozvannaya,M., Pivorunas,V.L., Feldman,Z. and Burton,B.M. (2013) SpoIIIE achieves directional DNA translocation through allosteric regulation of ATPase activity by an accessory domain. *J. Biol. Chem.*, **288**, 28962–28974.
46. Hopfner,K.P. and Michaelis,J. (2007) Mechanisms of nucleic acid translocases: lessons from structural biology and single-molecule biophysics. *Curr. Opin. Struct. Biol.*, **17**, 87–95.
47. Lakowicz,J.R. (2006) *Principles of Fluorescence Spectroscopy*. Springer, New York.
48. Sharp,M.D. and Poglano,K. (1999) An in vivo membrane fusion assay implicates SpoIIIE in the final stages of engulfment during *Bacillus subtilis* sporulation. *Proc. Natl Acad. Sci. USA*, **96**, 14553–14558.
49. Deyrup,A.T., Krishnan,S., Cockburn,B.N. and Schwartz,N.B. (1998) Deletion and site-directed mutagenesis of the ATP-binding motif (P-loop) in the bifunctional murine ATP-sulfurylase/adenosine 5'-phosphosulfate kinase enzyme. *J. Biol. Chem.*, **273**, 9450–9456.
50. Lewis,R., Durr,H., Hopfner,K.P. and Michaelis,J. (2008) Conformational changes of a Swi2/Snf2 ATPase during its mechano-chemical cycle. *Nucleic Acids Res.*, **36**, 1881–1890.
51. Monod,J., Wyman,J. and Changeux,J.-P. (1965) On the nature of allosteric transitions: A plausible model. *J. Mol. Biol.*, **12**, 88–118.
52. Levitzki,A. and Schlessinger,J. (1974) Cooperativity in associating proteins. Monomer-dimer equilibrium coupled to ligand binding. *Biochemistry*, **13**, 5214–5219.
53. Brown,B.M., (1994) P22 Arc: energetics and cooperativity of DNA binding, PhD thesis, Massachusetts Institute of Technology.
54. Gogol,E.P., Seifried,S.E. and von Hippel,P.H. (1991) Structure and assembly of the *Escherichia coli* transcription termination factor rho and its interaction with RNA. I. Cryoelectron microscopic studies. *J. Mol. Biol.*, **221**, 1127–1138.
55. Skordalakes,E. and Berger,J.M. (2003) Structure of the Rho transcription terminator: mechanism of mRNA recognition and helicase loading. *Cell*, **114**, 135–146.
56. Burton,B.M., Marquis,K.A., Sullivan,N.L., Rapoport,T.A. and Rudner,D.Z. (2007) The ATPase SpoIIIE transports DNA across fused septal membranes during sporulation in *Bacillus subtilis*. *Cell*, **131**, 1301–1312.
57. Marquis,K.A., Burton,B.M., Nollmann,M., Ptacin,J.L., Bustamante,C., Ben-Yehuda,S. and Rudner,D.Z. (2008) SpoIIIE strips proteins off the DNA during chromosome translocation. *Genes Dev.*, **22**, 1786–1795.